BIOCHEMISTRY

Splitting of the O–O bond at the heme-copper catalytic site of respiratory oxidases

Federica Poiana,[1] Christoph von Ballmoos,[2] Nathalie Gonska,[1] Margareta R. A. Blomberg,[3] Pia Ädelroth,[1] Peter Brzezinski[1]*

Heme-copper oxidases catalyze the four-electron reduction of O_2 to H_2O at a catalytic site that is composed of a heme group, a copper ion (Cu_B), and a tyrosine residue. Results from earlier experimental studies have shown that the O–O bond is cleaved simultaneously with electron transfer from a low-spin heme (heme a/b), forming a ferryl state (P_R; $Fe^{4+}{=}O^{2-}$, Cu_B^{2+}–OH^-). We show that with the *Thermus thermophilus* ba_3 oxidase, at low temperature (10°C, pH 7), electron transfer from the low-spin heme b to the catalytic site is faster by a factor of ~10 ($\tau \cong 11$ µs) than the formation of the P_R ferryl ($\tau \cong 110$ µs), which indicates that O_2 is reduced before the splitting of the O–O bond. Application of density functional theory indicates that the electron acceptor at the catalytic site is a high-energy peroxy state [Fe^{3+}–O^-–$O^-(H^+)$], which is formed before the P_R ferryl. The rates of heme b oxidation and P_R ferryl formation were more similar at pH 10, indicating that the formation of the high-energy peroxy state involves proton transfer within the catalytic site, consistent with theory. The combined experimental and theoretical data suggest a general mechanism for O_2 reduction by heme-copper oxidases.

INTRODUCTION

Cytochrome c oxidase (CytcO) catalyzes the reduction of O_2 to H_2O in the respiratory chain of aerobic organisms using reduced cytochrome (cyt.) c as an electron donor. The enzyme is a transmembrane protein that is composed of two or more subunits, which harbor four redox-active metal sites. During turnover, electrons from cyt. c are transferred first to the primary electron acceptor Cu_A, then to the low-spin heme intermediate electron acceptor, and finally to the catalytic site, which consists of a heme group and a copper ion, Cu_B, in close proximity, as well as a redox-active Tyr residue (Fig. 1) [for a review of the structure and function of oxidases, see related studies (*1*–*14*)]. The heme-copper oxidases typically pump, on average, 0.5 to 1 proton across the membrane per electron transferred from cyt. c to the catalytic site.

The oxidases are classified based on their structural details, particularly the architecture of the proton pathways, as members of one of three classes denoted by letters A, B, and C (*15*–*17*). The type of heme groups varies in different oxidases, and it is not strictly related to the class of the CytcO. In the B-type CytcO from *Thermus thermophilus*, the low-spin intermediate electron acceptor is heme b, whereas heme a_3 resides in the catalytic site; that is, the CytcO is a cyt. ba_3. The well-studied A-type CytcOs from *Rhodobacter sphaeroides*, *Paracoccus denitrificans*, and mitochondria are all aa_3 CytcOs.

The A-family bacterial oxidases use two proton pathways starting at the surface on the negative (n) side of the membrane, namely, the K and D pathways. The ba_3 CytcO from *T. thermophilus* harbors only one functional proton pathway (*18*), which approximately overlaps in space with the K pathway in the A-type oxidases, and it is therefore referred to as the K pathway analog. Structures of the ba_3 CytcO have been determined at atomic resolution using x-ray crystallography (*19*–*21*).

Detailed kinetic and mechanistic information for the *T. thermophilus* ba_3 CytcO has been obtained, for example, from studies of the reaction of the reduced CytcO with O_2 and the comparison of this reaction sequence to that in the well-studied A-type oxidases. With the A-type oxidases, dioxygen binds first to heme a_3 at the catalytic site, forming the oxo-ferrous intermediate called **A**, first described by Chance *et al.* (*22*). It was assumed originally that after O_2 binding to CytcO, a peroxy intermediate (Eq. 1) is formed at heme a_3 [see related studies (*23*–*26*)]

$$[Fe_{a3}^{2+} - O_2] + Cu_B^+ + e^- + H^+ \rightarrow [Fe_{a3}^{3+} - O^- - O^-(H^+)] + Cu_B^+ \quad (1)$$

Hence, this state was referred to as **P**. However, on the basis of an analysis of the optical absorption spectra of the **P** state, Weng and Baker (*27*) suggested that the O–O bond is broken in the **P** state, indicating that a ferryl state ($Fe_{a3}^{4+}{=}O^{2-}$) is formed (Eq. 2). Further support for this suggestion was obtained from resonance Raman experiments (*28*–*31*). In 1999, Fabian *et al.* (*32*) demonstrated that one of the oxygen atoms of the O_2 molecule bound to the two-electron reduced CytcO was released to solvent, which was interpreted to show that the O–O bond is broken upon formation of **P**

$$[Fe_{a3}^{2+} - O_2] + Cu_B^+ + e^- + H^+ \rightarrow [Fe_{a3}^{4+} = O^{2-}] + [Cu_B^{2+} - OH^-] \quad (2)$$

The source of the electron and proton at the left-hand side of the reaction varies depending on the initial state of the CytcO. If only the catalytic site is reduced, then the electron and proton are transferred from a Tyr residue (Tyr^{288} or Tyr^{237} in *R. sphaeroides* aa_3 CytcO or *T. thermophilus* ba_3 CytcO, respectively) (*26*, *29*, *33*–*35*), which forms a tyrosyl radical, TyrO•. The state that is formed is denoted $\mathbf{P_M}$ (Eq. 3)

$$[Fe_{a3}^{2+} - O_2] + Cu_B^+ + TyrOH \rightarrow [Fe_{a3}^{4+} = O^{2-}] + [Cu_B^{2+} - OH^-] + TyrO^\bullet \quad (3)$$

The time constant of this reaction is 200 to 300 µs (*36*, *37*), and the $\mathbf{P_M}$ state is stable over a time scale of minutes (*38*).

[1]Department of Biochemistry and Biophysics, Arrhenius Laboratories for Natural Sciences, Stockholm University, SE-106 91 Stockholm, Sweden. [2]Department of Chemistry and Biochemistry, University of Bern, 3012 Bern, Switzerland. [3]Department of Organic Chemistry, Arrhenius Laboratories for Natural Sciences, Stockholm University, SE-106 91 Stockholm, Sweden.
*Corresponding author. Email: peterb@dbb.su.se

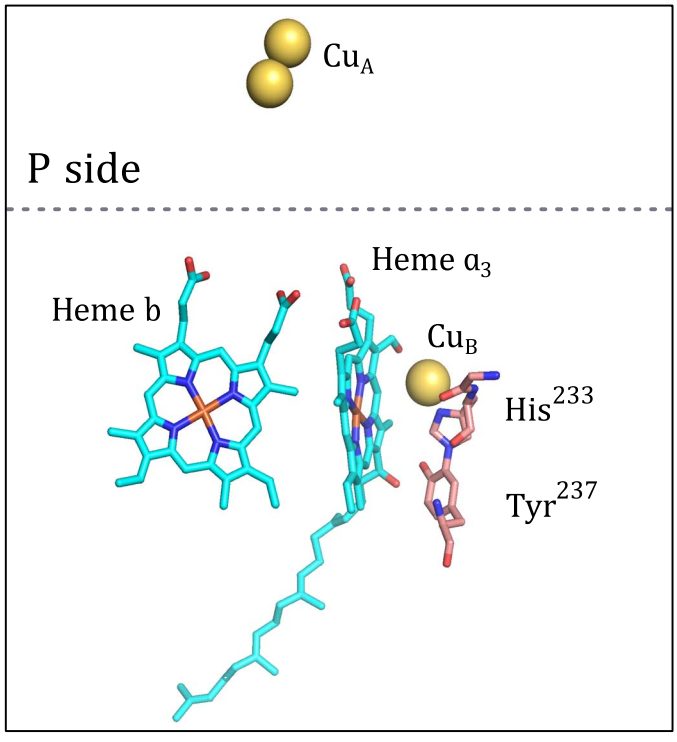

Fig. 1. Structure of the catalytic site. The redox-active cofactors of cyt. ba$_3$. The low-spin heme b and heme a$_3$ are depicted in cyan; Cu$_B$ and the dinuclear Cu$_A$ are indicated by yellow spheres. The cross-linked residues His^{233} and Tyr^{237}, located in proximity of the catalytic site, are shown. The image was prepared using the software PyMOL [Protein Data Bank code 3S8F (*20*)]. The dashed line is the approximate position of the membrane surface on the positive (p) side of the membrane.

When the **P** state is formed in the fully reduced CytcO, the electron is transferred from the low-spin heme a iron (Fe_a^{2+}), and the Tyr residue donates only a proton. The state is referred to as $\mathbf{P_R}$ (Eq. 4)

$$[Fe_{a3}^{2+} - O_2] + Cu_B^{+} + TyrOH + Fe_a^{2+} \rightarrow [Fe_{a3}^{4+} = O^{2-}] + [Cu_B^{2+} - OH^{-}] + TyrO^{-} + Fe_a^{3+} \quad (4)$$

The $\mathbf{P_R}$ formation time constants were found in the range 30 to 70 μs (*37*, *39*–*44*), depending on the species from which the CytcO is isolated.

The summary above shows that the $\mathbf{P_M}$ and $\mathbf{P_R}$ states have the same structure; the only difference is the donor of the "fourth" electron, which is Tyr^{288} or the low-spin heme, respectively [reviewed by Kaila *et al.* (*9*)]. Note that the formation of $\mathbf{P_M}$/$\mathbf{P_R}$ is not associated with any proton uptake from the solution to the catalytic site (*45*–*47*); the Tyr residue is the hydrogen or proton donor.

Although a peroxy state [Fe^{3+}–O^-–O^-(H^+)] has not been previously observed upon reaction of the reduced CytcO with O_2, on the basis of theoretical studies, it has been predicted that this state (called $\mathbf{I_P}$) is formed transiently on the reaction path leading from state **A** to state $\mathbf{P_M}$ (*48*–*50*). $\mathbf{I_P}$ has not been observed because it is higher in energy than state **A**. Here, we investigated the formation of the $\mathbf{P_R}$ state in the *T. thermophilus* ba$_3$ CytcO as a function of temperature at neutral and high pH (10). The data indicate that at neutral pH and low temperature (10°C), electron transfer from heme b to the catalytic site is about 10 times faster than the formation of the $\mathbf{P_R}$ state, which suggests that a true peroxy state is formed transiently before the O–O bond is broken in $\mathbf{P_R}$. This difference in rate constants was not observed at higher temperatures (~45°C), where the electron transfer and $\mathbf{P_R}$ formation displayed the same rate constants, just as in the A-type CytcOs at room temperature. Furthermore, at high pH (10), the difference in rate constants (at low temperature) was significantly smaller than at neutral pH, which suggests that formation of a transient peroxy state [Fe^{3+}–O^-–O^-(H^+)] involves internal proton transfer within the catalytic site.

RESULTS

Experimental results

The reduced cyt. ba$_3$ CytcO, with CO bound to heme a$_3$, was mixed with an O_2-saturated solution after which the CO ligand was removed by means of a laser flash to allow O_2 to bind to heme a$_3$. Absorbance changes were monitored at 560 and 610 nm. At 560 nm, there is a maximum in the contribution of the redox changes of heme b, whereas at 610 nm, the binding of O_2 and the formation of the "peroxy" (P) intermediate are observed [a broad trough near 615 nm and a peak at 610 to 612 nm (*51*, *52*)]. Figure 2 shows absorbance changes as a function of time after CO dissociation at $t = 0$. The starting level of the traces just after the flash (adjusted to zero) reflects the absorbance of the reduced CytcO relative to that of the CytcO-CO complex.

We first discuss data at 10°C and pH 7. At 610 nm (Fig. 2A), the first decrease in absorbance is associated with the binding of O_2 to heme a$_3$ with a rate constant of $2.8 \times 10^5 \pm 0.8 \times 10^5$ s^{-1} ($\tau \cong 3.6$ μs). The increase in absorbance is associated with the formation of the $\mathbf{P_R}$ state with a rate constant of $9 \times 10^3 \pm 1 \times 10^3$ s^{-1} ($\tau \cong 110$ μs), whereas the slowest decrease in absorbance is associated with oxidation of the CytcO with a rate constant of 400 ± 60 s^{-1} ($\tau \cong 2.5$ ms). At 560 nm (Fig. 2A), the initial decrease in absorbance is associated with oxidation of heme b with a rate constant of $9 \times 10^4 \pm 4 \times 10^4$ s^{-1} ($\tau \cong 11$ μs), which is followed in time by re-reduction of heme b ($\tau = 180 \pm 30$ μs) and oxidation ($\tau = 2.6 \pm 0.2$ ms). The data indicate that at 10°C and pH 7, oxidation of heme b (decrease in absorbance at 560 nm, $\tau \cong 11$ μs) was ~10 times faster than the formation of state $\mathbf{P_R}$ (increase in absorbance at 610 nm, $\tau \cong 110$ μs).

At high temperature (45°C) and pH 7 (Fig. 2B), the decrease in absorbance at 560 nm (oxidation of heme b) and the increase in absorbance at 610 nm (formation of $\mathbf{P_R}$) displayed rate constants of $1.9 \times 10^5 \pm 0.2 \times 10^5$ s^{-1} ($\tau \cong 5.3$ μs) and $1.5 \times 10^5 \pm 0.5 \times 10^5$ s^{-1} ($\tau \cong 6.7$ μs), respectively, that is, the same within the error. Figure 2 (C and D) shows absorbance changes at pH 10 and at 10° and 45°C, respectively. At higher pH, the ratios of the rate constants of heme b oxidation and $\mathbf{P_R}$ formation were ~3 and ~1.3 at 10° and 45°C (the rate constant values are given in Table 1), respectively; that is, the difference in rates at a low temperature was smaller than at neutral pH.

Figure 3A shows the temperature dependence of the rate constant for the absorbance change attributed to $\mathbf{P_R}$ formation at 610 nm (black trace) and those attributed to heme b oxidation at 560 nm (red trace) at pH 7. As seen in the figure, the difference between these rate constants was significantly larger at low than at high temperature. Figure 3 also shows the temperature dependence of the kinetic component associated with the binding of O_2 (blue trace, $\tau = 2$ to 4 μs). This time constant was essentially temperature-independent, presumably because the slower O_2 binding at lower temperatures is compensated for by the increased solubility of O_2.

Figure 4 shows absorbance changes at 610 nm associated with the reaction of the mixed-valence ba$_3$ CytcO (that is, reduced heme a$_3$ and

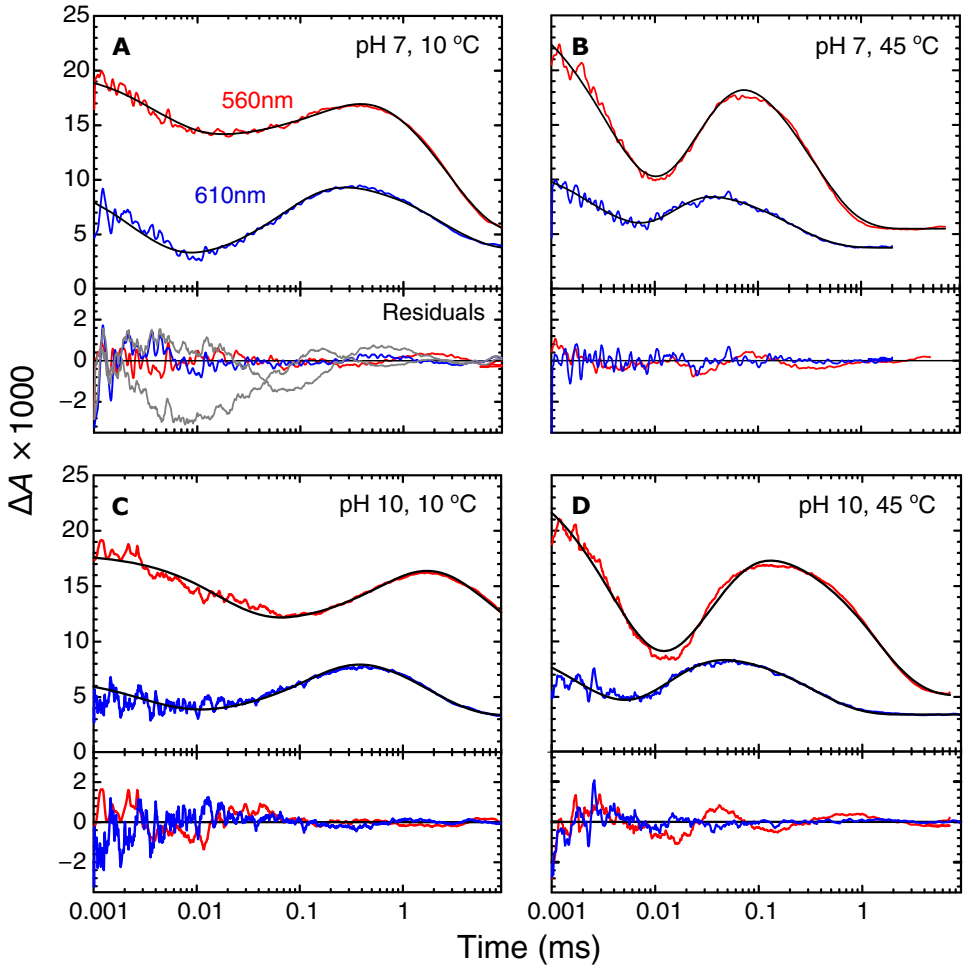

Fig. 2. Absorbance changes during reaction of the fully reduced ba_3 CytcO with O_2. (**A** and **B**) pH 7 at 10° and 45°C, respectively. (**C** and **D**) pH 10 at 10° and 45°C, respectively. At 610 and 560 nm, the absorbance changes are mainly attributed to redox changes at heme a_3 and heme b, respectively. The black lines are fits of the data with a model that is described by a sum of three exponential functions. The rate constants obtained from the fit are given in the text and in Table 1. The difference between the fit and the data (that is, the residuals) is shown below each panel. In addition, in (A), we show the residuals of a fit with a single rate constant (5×10^4 s^{-1}) for electron transfer from heme b to the catalytic site and $\mathbf{P_R}$ formation (gray lines). Experimental conditions after mixing: 0.6 to 0.8 μM CytcO (scaled to 1 μM), 0.05% DDM, 90 mM Hepes (pH 7) or 90 mM CAPS (pH 10), and ~1 mM O_2. The cuvette path length was 1.00 cm. The 560-nm traces are shifted up by 1.7×10^{-3} units for clarity.

Table 1. Rate constants for the early steps of O_2 reduction at low and high temperature for pH 7 and 10, respectively. Errors are the SDs for $n = 3$ (pH 10 data) or $n = 4$ (pH 7 data) measurements.

		Rate constant (s^{-1}) (Time constant) (μs)	
	T **(°C)**	**pH 7**	**pH 10**
O_2 binding (610-nm decay)	10	$(2.8 \pm 0.8) \times 10^5$ (3.6)	$(2.9 \pm 0.1) \times 10^5$ (3.4)
	45	$(2.7 \pm 0.8) \times 10^5$ (3.7)	$(4 \pm 1) \times 10^5$ (2.5)
Heme b oxidation (k_b) (560-nm decay)	10	$(9 \pm 4) \times 10^4$ (11)	$(2.6 \pm 0.6) \times 10^4$ (38)
	45	$(1.9 \pm 0.2) \times 10^5$ (5.3)	$(1.9 \pm 0.2) \times 10^5$ (5.3)
P_R formation (k_P) (610-nm increase)	10	$(9 \pm 1) \times 10^3$ (110)	$(8.7 \pm 0.3) \times 10^3$ (120)
	45	$(1.8 \pm 0.5) \times 10^5$ (5.5)	$(1.5 \pm 0.5) \times 10^5$ (6.7)
Ratio (k_b/k_P)	10	10	3
	45	1.1	1.3

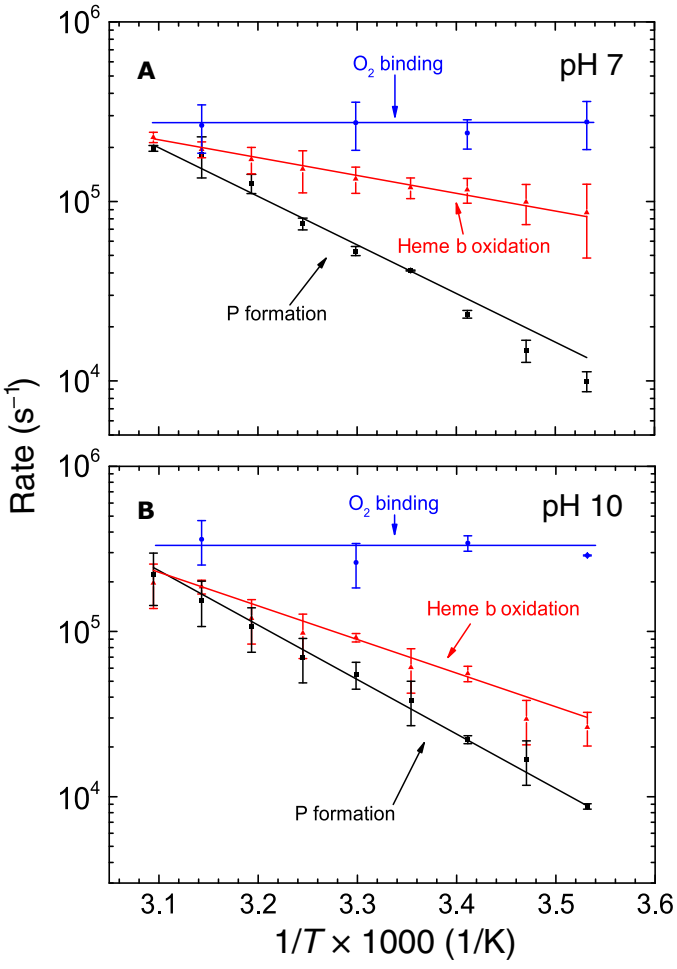

Fig. 3. Temperature dependence of the rate constants. The rates of O_2 binding (Arrhenius plots), heme b oxidation, and $\mathbf{P_R}$ formation are shown as indicated in the graphs for (**A**) pH 7 and (**B**) pH 10. Conditions were the same as in Fig. 2.

Cu_B and oxidized heme b and Cu_A) with O_2 at ~22°C and neutral pH. The increase in absorbance is associated with the formation of the $\mathbf{P_M}$ state with a rate constant of $7.1 \times 10^3 \pm 0.7 \times 10^3$ s^{-1} ($\tau \cong 140$ μs), consistent with results from earlier studies (*36*, *37*). The rate constant of this reaction is pH-independent in the pH range 6.1 to 9.2 (*53*), and it is not associated with proton uptake from the solution (*46*).

Computation results

Previous computational studies (see Introduction), have suggested a two-step mechanism for the O–O bond cleavage upon reaction of the two-electron reduced CytcO with O_2 (Fig. 5) (*48*, *50*). Starting from state **A**, in the first step, a proton is transferred from Tyr^{237} (see Fig. 1) to the oxygen molecule, together with two electrons (one from the heme iron and one from either Cu_B or Tyr), resulting in the formation of a Fe^{3+}–O^-–$O^-(H^+)$ peroxide intermediate ($\mathbf{I_P}$). In the second step (dashed line), the O–O bond is cleaved, forming state $\mathbf{P_M}$, with a hydroxyl group on Cu_B and a ferryl.

Considering the reaction of the four-electron reduced CytcO with O_2, when is the electron transferred from the low-spin heme b to the catalytic site? The present calculations show that the electron affinity of intermediate **A** is significantly lower than that of the electron donor heme b [also compare the study of Blomberg (*54*)], which is expected because there is no strong electron acceptor at the catalytic site. On the other hand, in the peroxide intermediate $\mathbf{I_P}$, an electron acceptor, either Cu^{2+} or the tyrosyl radical, is created, resulting in an increase of the calculated electron affinity by about ~50 kJ/mol (not shown in Fig. 5). This result indicates that the product of the electron transfer is a reduced peroxide intermediate, $\mathbf{I_P}^-$ (Fig. 5), that relaxes to $\mathbf{P_R}$ upon cleaving the O–O bond.

The transition state for O–O bond cleavage ($\mathbf{TS_{O-O}}$) was determined for both $\mathbf{I_P}$ and $\mathbf{I_P}^-$ intermediates. The calculated barrier heights are quite similar, 38.5 and 36.8 kJ/mol, respectively (from $\mathbf{I_P}$ and $\mathbf{I_P}^-$, respectively, to $\mathbf{TS_{O-O}}$ in Fig. 5). The rate constants for $\mathbf{P_R}$ and $\mathbf{P_M}$ formation are determined by the energy difference between intermediate **A** and the highest point on the energy profiles. A transition state was determined for the initial proton transfer step ($\mathbf{TS_H}$), but because the calculated barrier height depends on the number of water molecules included in the model, a definite value could not be determined. However, it is estimated that $\mathbf{TS_H}$ is similar to or lower than $\mathbf{TS_{O-O}}$, and therefore, the position of $\mathbf{TS_{O-O}}$ (that is, the highest point) determines the formation rate constant of both $\mathbf{P_R}$ and $\mathbf{P_M}$. The height of this rate-limiting barrier is the sum of the endergonicity for the formation of the peroxide intermediate ($\mathbf{I_P}$ or $\mathbf{I_P}^-$) and the O–O bond cleavage barrier relative to the peroxide.

Using the present model without considering any charges in the K pathway, we found the peroxide intermediate $\mathbf{I_P}$ to be 30.5 kJ/mol above intermediate **A** (this level is not shown in Fig. 5), which would lead to a total barrier for $\mathbf{P_M}$ formation of almost 70 kJ/mol. This is much higher than the activation free energy of about 50 kJ/mol, corresponding to the experimentally observed rate constant. Therefore, in previous computational studies, we investigated factors that could influence the barrier height. In particular, it was shown that a positive charge, for example, at Lys^{362} of the *R. sphaeroides* CytcO (*55*), in the vicinity of the negatively charged tyrosinate, significantly stabilizes the peroxide intermediate $\mathbf{I_P}$ relative to **A** (*48*, *50*). Therefore, it can be suggested that the positive charge would yield an estimated difference between $\mathbf{I_P}$ and **A**, as shown in Fig. 5, yielding an overall barrier of about 50 kJ/mol for $\mathbf{P_M}$ formation (highest barrier from **A** to $\mathbf{P_M}$; see Fig. 5). Note as well that with the smaller energy difference between **A** and $\mathbf{I_P}$, the latter would remain unobservable (populated to ~5%), in agreement with the experiments. Furthermore, the calculated electron affinity of intermediate $\mathbf{I_P}$ is similar to the calculated electron affinities of other intermediates of the catalytic cycle, which precede electron transfer to the catalytic site (*54*). Hence, it is reasonable to assume that the electron transfer step to form state $\mathbf{I_P}^-$ is somewhat exergonic, putting this state close enough in energy to intermediate **A** to become observable, in accordance with the present experiments (see Fig. 5). Because the O–O bond cleavage barrier relative to the preceding peroxide state is rather similar for $\mathbf{I_P}$ and $\mathbf{I_P}^-$ (see above), the difference in rate constants for $\mathbf{P_M}$ and $\mathbf{P_R}$ formation is mainly the result of the exergonicity of the electron transfer from heme b to $\mathbf{I_P}$, forming $\mathbf{I_P}^-$. In summary, the qualitative picture of the O–O bond cleavage step obtained from the quantum chemical calculations is used to construct the energy profiles presented in Fig. 5, wherein the detailed relative energies are adapted to fit the present experimental data at low temperatures and neutral pH.

DISCUSSION

As described in detail in the Introduction, early models assumed that immediately after O_2 binding to heme a_3, a peroxy state is formed,

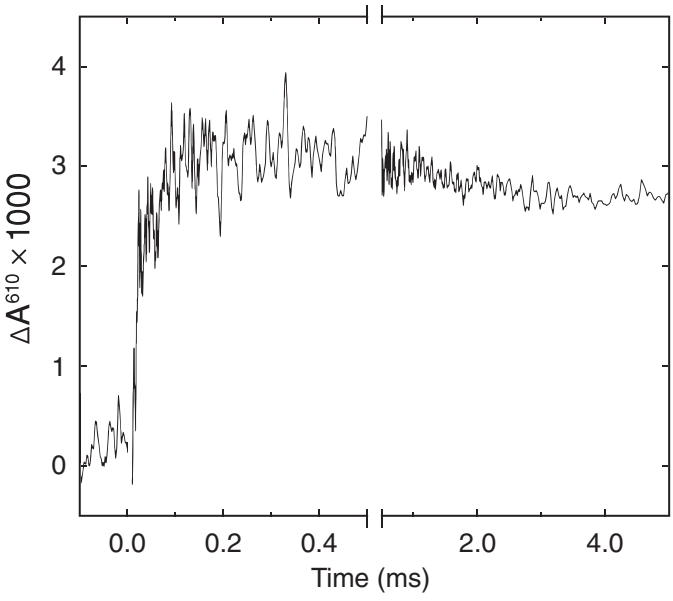

Fig. 4. Kinetics of the reaction of mixed-valence CytcO with O_2. The reaction was monitored at 610 nm. Experimental conditions after mixing: 0.6 to 0.8 μM CytcO (scaled to 1 μM), 0.05% DDM, and 90 mM Hepes (pH 7.4). A laser artifact at t = 0 has been truncated for clarity.

which is the first reaction intermediate that is experimentally observed. Accordingly, this state was called **P**. Results from studies done after 1990 indicate that the O–O bond is already broken in the **P** state.

In an earlier study with the *T. thermophilus* ba_3 CytcO, we noted that oxidation of heme b (absorbance decrease at 560 nm) was slightly faster than formation of $\mathbf{P_R}$ (absorbance increase at 610 nm) at ambient temperatures (*56*), but the difference was not sufficiently large to be discussed in depth at that time. Furthermore, on the basis of results obtained earlier with the A-type CytcO, we assumed that heme b oxidation and $\mathbf{P_R}$ formation should display the same rate constants, and therefore, in the model, both processes were fitted to the same transition rate constant. Here, we observed that the difference in rate constants is significantly more pronounced at low temperatures, where, at 10°C (pH 7), oxidation of the low-spin heme b occurs faster by a factor of ~10 than formation of the $\mathbf{P_R}$ state; that is, it was not possible to fit the two processes to the same rate constant (see residuals in Fig. 2A). This relatively large difference in rate constants also allowed us to separately determine the temperature dependence of each process (Fig. 3).

The O_2 binding is slightly faster than that previously observed (*51*) (5.3 μs) and falls between the values obtained by Szundi *et al.* (*57*) (~1 or ~10 μs), depending on experimental conditions. Using a slightly different experimental approach, Szundi *et al.* (*57*) suggested that the CO ligand may interfere with O_2 binding, thereby slowing, for example, heme b oxidation by a factor of ~10, from 5 to 60 μs. As discussed previously (*56*), we did not observe this interference from CO dissociation.

The Arrhenius activation energy for $\mathbf{P_R}$ formation in the *R. sphaeroides* CytcO is ~20 kJ/mol (*37*), that is, lower than that for $\mathbf{P_R}$ formation with the ba_3 CytcO but about the same as that for heme b oxidation (see Table 2). In earlier studies, the value for another transition (**F→O**) was determined [~42 kJ/mol (*58*)]. This reaction involves both electron transfer from heme b to the catalytic site and proton transfer from the solution. Previous experience has shown that the type of computational studies used in this study to interpret the data yields better agreement with the experiment for free energies than for the partitioning into enthalpy and entropy contributions, which may be related to the fact that the source for this partitioning is not always located in the active site (*49*, *59*). Therefore, we present the parameters in Table 2 without further discussion.

When heme b becomes oxidized before state $\mathbf{P_R}$ is formed, a question regarding the identity of the electron acceptor arises. Upon binding of O_2, that is, forming of state **A**, in the fully reduced CytcO, none of the redox sites can accept any additional electrons. State $\mathbf{P_R}$ is formed over a time scale of 110 μs at 10°C (Fig. 2A and Table 1). Consequently, if $\mathbf{P_R}$ was the first intermediate to be formed at the catalytic site after binding of O_2 (intermediate **A**), there would be no available electron acceptor over the time scale wherein we observed oxidation of heme b ($\tau \cong 11$ μs at 10°C; see Fig. 2A). The $\mathbf{P_M}$ state was formed with a time constant of ~140 μs at ~20°C (Fig. 4); that is, this state was not formed before electron transfer from heme b. To explain the data, we must therefore consider mechanisms to create an electron acceptor after binding of O_2 but before breaking of the O–O bond. One plausible possibility is to form a transient peroxy intermediate over the same time scale as electron transfer from heme b. This intermediate was suggested by Blomberg *et al.* (*48*–*50*), and a reaction scheme including this state ($\mathbf{I_P}$) is presented in Fig. 5. The absorbance change associated with the $\mathbf{A \rightarrow I_P^-}$ reaction would then correspond to the difference between states heme b^{2+} Fe^{2+}–O_2 and heme b^{3+} Fe^{3+}–O^-–$O^-(H^+)$, which would be dominated by the absorbance change associated with oxidation of heme b. This is because the O–O bond length in state Fe^{2+}–O_2 is in between that of dioxygen and peroxide, similar to a superoxide coordinated to a ferric iron (Fe^{3+}–O_2^-) (*60*), and we assume that no major absorbance changes occur at heme a_3 during the transition from a superoxide-like state to a peroxy state.

According to the theoretical model (*48*–*50*), in state $\mathbf{I_P}$, the heme a_3 iron is oxidized and an electron is transferred to O_2 from either Cu_B or Tyr^{237}, wherein the latter in both cases is also the proton donor (Fig. 5). In the absence of an electron at heme b, state $\mathbf{I_P}$ would relax to $\mathbf{P_M}$. However, if heme b is reduced, as in our experiments, then the formation of $\mathbf{I_P}$ would be accompanied by electron transfer from heme b to the catalytic site, forming state $\mathbf{I_P^-}$, which is lower in energy than $\mathbf{I_P}$. In this model, observation of $\mathbf{I_P^-}$ is possible only if the energy level of this state is sufficiently close to that of state **A**. As outlined in Results, the time constant for the overall $\mathbf{A \rightarrow P_{R/M}}$ reaction is dependent on the energy difference between state **A** and the highest transition state $\mathbf{TS_{O-O}}$ (Fig. 5). Because $\mathbf{I_P^-}$ is lower in energy than $\mathbf{I_P}$ and the energy difference between $\mathbf{I_P}$ and $\mathbf{TS_{O-O}}$ is approximately the same as that between $\mathbf{I_P^-}$ and $\mathbf{TS_{O-O}}$, the highest energy barrier along the trajectory from **A** to $\mathbf{P_R}$ is lower than that leading to $\mathbf{P_M}$. This difference explains why the formation of $\mathbf{P_R}$ occurs over a shorter time scale than the formation of $\mathbf{P_M}$. Furthermore, according to the model, the $\mathbf{I_P}$ state would not be observed upon the reaction of the mixed-valence CytcO with O_2 because state $\mathbf{I_P}$ is higher in energy than $\mathbf{I_P^-}$; that is, with the mixed-valence CytcO, state $\mathbf{I_P}$ would not be populated.

Next, we discuss differences in the data obtained at pH 7 and 10, respectively. We note that at high pH, the rate constants of heme b oxidation and $\mathbf{P_R}$ formation displayed more similar slopes in the Arrhenius plots than at pH 7 (Fig. 3). The proposed model involves proton transfer from the Tyr residue to stabilize the peroxy state in $\mathbf{I_P}$ (Fig. 5) (*48*), which would also take place at high pH because the Tyr^{237} residue in the ba_3 CytcO is presumably protonated [for example, see the study of Koutsoupakis *et al.* (*52*)]. To explain the larger slope in the temperature dependence of heme b oxidation at high pH, we assume that the K pathway "below" Tyr^{237} becomes more negative (or less positive) upon increasing the pH. This change in the charge would stabilize the proton

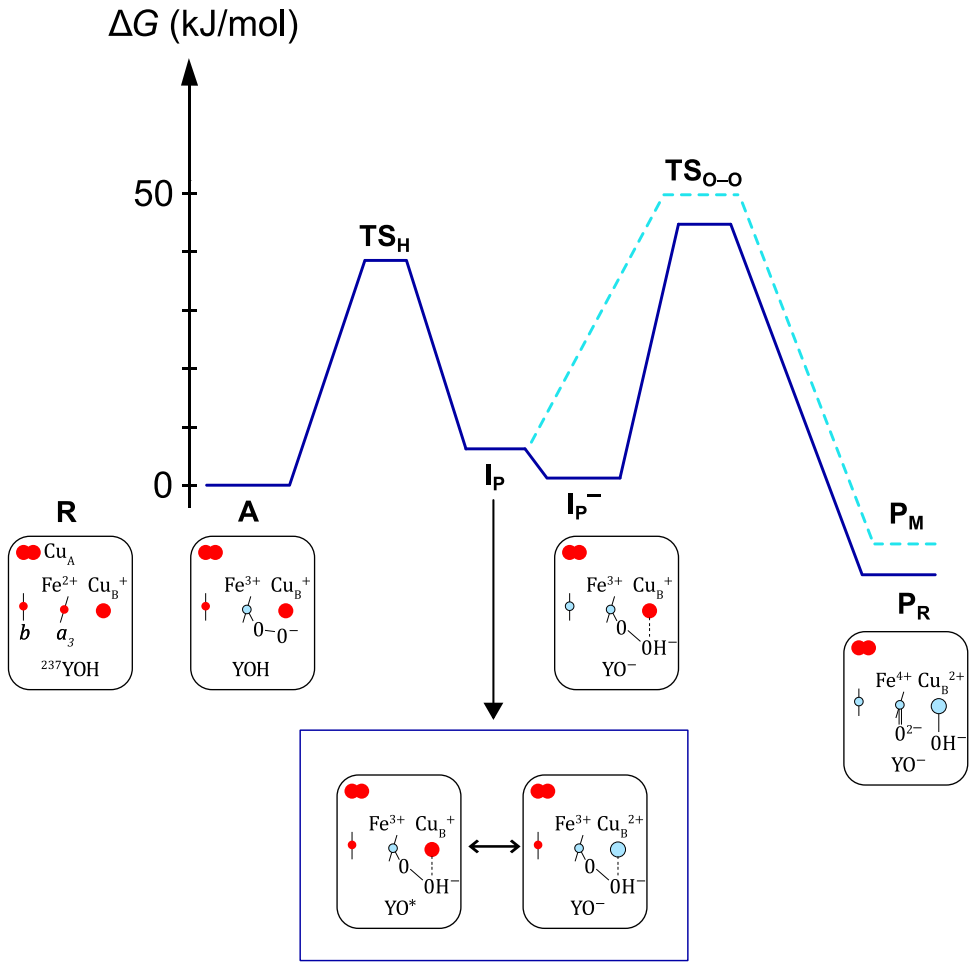

Fig. 5. Mechanism of the initial steps of O_2 reduction catalyzed by the ba_3 CytcO. Energy profiles for the initial reaction steps after binding of O_2 to heme a_3, reflecting the approximate rate constants observed at pH 7 and 10°C. The reduced CytcO (state **R**) binds O_2 to state **A**. In state $\mathbf{I_P}$, a peroxy state is formed upon oxidation of the heme a_3 iron and either Cu_B or Tyr^{237}. The peroxy state is stabilized by a proton from Tyr^{237}. The reaction sequence below the diagram illustrates the specific electron transfers within the ba_3 CytcO. Two possible configurations that are in resonance are shown for state $\mathbf{I_P}$. It is a geometric single minimum with an electronic structure that is a mixture (resonance) of two main electronic configurations.

Table 2. Thermodynamic parameters. The parameters were determined by fitting the data in Fig. 3 with the expression $k = A\ \exp(-E_a/RT)$. The range of *A* values was 30 to 40% of the values in the table (when taking into account the error bars in Fig. 3).

	pH 7		pH 10	
	E_a (kJ/mol)	ln *A*	E_a (kJ/mol)	ln *A*
Heme b oxidation (560-nm first decay)	17 ± 2	18	40 ± 4	27
P_R formation (610-nm increase)	60 ± 5	34	60 ± 5	34

at Tyr^{237} such that the height of the transition state $\mathbf{TS_H}$ would increase slightly at high pH. This change in the barrier height would act to slow the initial reaction step $\mathbf{A \rightarrow I_P}$. In the *T. thermophilus* ba_3 CytcO, which lacks a residue equivalent to Lys^{362}, the overall charge may be determined by the protonation state of several groups in the K pathway, including Tyr^{244}, Tyr^{248} (SU I), and Glu^{15} (SU II) (*18*, *52*, *61*, *62*).

Assuming that the suggested scenario is generally applicable for respiratory oxidases, the data from this study would point to a mechanism for the initial steps of O_2 reduction at the catalytic site: Electron transfer from the low-spin heme to the catalytic site would coincide with formation of a peroxy state, as originally suggested (*23*, *25*), but the peroxy state Fe^{3+}–O^-–$O^-(H^+)$ would only be formed transiently, and it would not always be observed. This is because the intermediate would be observed (that is, populated to a sufficient concentration) only if the energy level of $\mathbf{I_P^-}$ is sufficiently close to that of intermediate **A**, which may not be the case in all CytcOs.

A question then arises, why is the formation of the "true" peroxy state [Fe^{3+}–O^-–$O^-(H^+)$] observed in the ba_3 CytcO but has not been observed in earlier studies with the A-type CytcOs? One possible explanation is that structural differences in the K pathway, as discussed above, would lead to differences in the transition state $\mathbf{TS_H}$ (Fig. 5). Another possibility is that the different CytcOs are optimized to operate at different temperatures. With the ba_3 CytcO, electron transfer from heme b to the catalytic site and $\mathbf{P_R}$ formation are presumably synchronized at temperatures >45°C, but the different slopes in the temperature dependencies of the rate constants lead to a clear separation

in the rate constants at 10°C. Other A-type CytcOs are presumably optimized to operate at lower temperatures, and a separation of the two rate constants would be observed only at temperatures significantly lower than 10°C. In other words, we assume the same mechanism but slightly shifted relative energy levels in the diagram in Fig. 5 for the different CytcOs.

SUMMARY

Earlier theoretical studies predicted a high-energy peroxy state, $\mathbf{I_P}$ [Fe^{3+}–O^-–$O^-(H^+)$], formed along the reaction pathway leading to O–O bond breaking at the catalytic site of the heme-copper oxidases. Here, we showed that at low temperatures, with the ba_3 *T. thermophilus* CytcO, an electron acceptor is formed at the catalytic site after ~11 μs, before the O–O bond breaking ($\tau \cong 110$ μs). This electron acceptor is suggested to be the predicted $\mathbf{I_P}$ state, which, after electron transfer to the catalytic site (state $\mathbf{I_P}^-$), becomes significantly populated in the *T. thermophilus* CytcO at low temperature.

MATERIALS AND METHODS

Purification of ba_3 CytcO

T. thermophilus HB8 strain YC 1001 (with a deletion of the *cba* gene) was transformed with a plasmid encoding the ba_3 CytcO gene with a 7-His tag at the N terminus of subunit I and cultivated at 60°C with mild shaking (125 rpm), as described by Chen *et al.* (*63*) [see also the study of Keightley *et al.* (*64*)]. The harvested cells were suspended in 100 mM Hepes (pH 8) at a ratio of about 1:3, together with a small amount of deoxyribonuclease. The cells were broken using a constant flow cell disrupter at 190 MPa (Constant Systems). The protease inhibitor phenylmethylsulfonyl fluoride was added but after breaking the cells to avoid excessive foaming during the breaking procedure. The solution was centrifuged for 1 hour at 205,000*g* at 16°C. The pellet was homogenized in 50 ml of 50 mM Hepes (pH 8) and 2.5% Triton X-100 for each 10 g of cell membrane, and the sample was incubated overnight at 4°C. The sample was centrifuged for 1 hour at 170,000*g*, and the obtained supernatant was supplemented with 10 mM imidazole and loaded onto a prepacked 5-ml Ni–nitrilotriacetic acid affinity chromatography column equilibrated with 10 mM Hepes (pH 8), 150 mM NaCl, 10 mM imidazole, and 1% Triton X-100. After binding of the CytcO, the column was washed with 10 mM Hepes (pH 8), 150 mM NaCl, 40 mM imidazole, and 1% Triton X-100, until the solution passing through the column was clear. Elution of the enzyme was obtained with 10 mM Hepes (pH 8), 150 mM NaCl, 250 mM imidazole, and 1% Triton X-100. The brown elution fractions were pooled and dialyzed overnight at 4°C in 1 liter of 5 mM Hepes (pH 8) and 0.05% Triton X-100 first and then in 1 liter of 5 mM Hepes (pH 8) and 0.05% dodecyl-β-D-maltoside (DDM). The enzyme was stored in this last buffer at 4°C until use.

The concentration of heme a_3 was determined from the fully reduced minus oxidized absorption difference spectrum using the absorption coefficient $\varepsilon(613–658) = 6.3\ mM^{-1}\ cm^{-1}$. The concentration of heme b was calculated from the fully reduced spectrum using $\varepsilon(560–590) = 26\ mM^{-1}\ cm^{-1}$.

Flow-flash measurements

Purified ba_3 CytcO was diluted to a final concentration of ~10 μM with 5 mM Hepes and 0.05% DDM (pH 7.4) and placed in a Thunberg cuvette. The sample was made anaerobic on a vacuum line, and air was replaced for N_2. The CytcO was then reduced by 2 mM sodium ascorbate using 0.5 μM phenazine methosulfate as a mediator. Incubation under 150 kPa N_2 for approximately 1 hour led to the formation of the fully reduced state. Last, the atmosphere was exchanged for CO, and complete binding to the catalytic site was observed after ~20 min of incubation under 100 kPa CO.

The flow-flash measurements were performed using a modified stopped-flow setup (Applied Photophysics) (*65*, *66*). Briefly, the ba_3 CytcO was mixed at a ratio of 1:5 with oxygen-saturated buffer [100 mM Hepes and 0.05% DDM (pH 7) or 100 mM 3-(cyclohexylamino)-1-propanesulfonic acid (CAPS) and 0.05% DDM (pH 10)]. After ~30 ms, a 10-ns laser flash (200 mJ, 532 nm; Nd-YAG laser Quantel) was used to dissociate the CO ligand, which initiated the catalytic reaction. Absorbance changes were monitored at specific wavelengths (see text and figure legends). The temperature in the optical chamber was varied using a thermostated water bath.

To prepare the mixed-valence CytcO, the oxidized CytcO [~10 μM in 5 mM Hepes (pH 7.4) and 0.05% DDM] was transferred to a Thunberg cuvette, after which air was replaced by N_2. Next, the gas was exchanged for CO, after which the sample was incubated for 2 to 3 hours. Formation of the mixed valence state was confirmed from the optical absorption spectrum (oxidized heme b and reduced heme a_3).

Data handling and analysis

The data were collected using a digital oscilloscope in which 10^7 sampling points were averaged to ~10^3 points using a pseudo-logarithmic oversampling function available in the LKS software (Applied Photophysics). If necessary, the traces were smoothed by averaging nine points in a moving time window. Data points in the time window 0 to 1 μs were removed to facilitate the analysis by eliminating a laser artifact (because of incomplete shielding of the detector from the laser flash). The signals were fitted to a model describing irreversible, sequential reactions using KinTek software (KinTek Corp.).

Computational details

Density functional theory was used to study the O–O bond cleavage in CytcO. The same model and methodology were used as those described by Blomberg and Siegbahn (*67*). The model of the catalytic site was based on the crystal structure of CytcO from *R. sphaeroides* (*1*). It contained heme a_3 and the Cu_B complex, including the cross-linked tyrosine. This part of the catalytic site is very similar to that of the ba_3 CytcOs, which means that the same model could be used to describe the details of the O–O bond cleavage step in both systems. The hybrid density functional B3LYP*-D3 [with 15% exact exchange and dispersion correction (*68*–*70*)] was used together with a polarized double zeta basis set (lacvp*) for the geometry optimizations and together with the large cc-pvtz(–f) basis plus lacv3p+ for the metals for the energy calculations (*71*). Polarizing effects from the surrounding protein were included using the self-consistent reaction field approach, and zero-point corrections to the energies were obtained from Hessian calculations. Entropy effects on the relative energies were found to be negligible for the investigated part of the reaction. For details on the model and the methods, see the study of Blomberg and Siegbahn (*67*). As previously noted (*54*), the computational results yield a qualitative picture of the reaction mechanism. In particular, spin states and redox properties of heme groups may not be correctly reproduced by density functional theory. Another difficulty concerns the description of water molecules in the catalytic site. The number and positions of water molecules seen in the crystal structures of the catalytic

site vary for the different CytcOs. Because this situation is difficult to handle computationally, the most accurate relative energies are obtained when no water molecules are included in the model. An obvious exception is the investigation of proton transfer reactions, where water molecules need to be included in the model. To obtain a more quantitative picture of the energetics of a reaction mechanism, a careful combination of computational and experimental results has to be used (*54*, *72*).

REFERENCES AND NOTES

1. J. P. Hosler, S. Ferguson-Miller, D. A. Mills, Energy transduction: Proton transfer through the respiratory complexes. *Annu. Rev. Biochem.* **75**, 165–187 (2006).
2. S. Yoshikawa, K. Muramoto, K. Shinzawa-Itoh, H. Aoyama, T. Tsukihara, K. Shimokata, Y. Katayama, H. Shimada, Proton pumping mechanism of bovine heart cytochrome *c* oxidase. *Biochim. Biophys. Acta* **1757**, 1110–1116 (2006).
3. A. Namslauer, P. Brzezinski, Structural elements involved in electron-coupled proton transfer in cytochrome *c* oxidase. *FEBS Lett.* **567**, 103–110 (2004).
4. P. Brzezinski, R. B. Gennis, Cytochrome c oxidase: Exciting progress and remaining mysteries. *J. Bioenerg. Biomembr.* **40**, 521–531 (2008).
5. P. Brzezinski, P. Ädelroth, Design principles of proton-pumping haem-copper oxidases. *Curr. Opin. Struct. Biol.* **16**, 465–472 (2006).
6. O.-M. H. Richter, B. Ludwig, Electron transfer and energy transduction in the terminal part of the respiratory chain—Lessons from bacterial model systems. *Biochim. Biophys. Acta* **1787**, 626–634 (2009).
7. S. Ferguson-Miller, C. Hiser, J. Liu, Gating and regulation of the cytochrome c oxidase proton pump. *Biochim. Biophys. Acta* **1817**, 489–494 (2012).
8. P. R. Rich, A. Maréchal, Functions of the hydrophilic channels in protonmotive cytochrome *c* oxidase. *J. R. Soc. Interface* **10**, 183–196 (2013).
9. V. R. I. Kaila, M. I. Verkhovsky, M. Wikström, Proton-coupled electron transfer in cytochrome oxidase. *Chem. Rev.* **110**, 7062–7081 (2010).
10. A. A. Konstantinov, Cytochrome *c* oxidase: Intermediates of the catalytic cycle and their energy-coupled interconversion. *FEBS Lett.* **586**, 630–639 (2012).
11. M. R. A. Blomberg, P. E. M. Siegbahn, Proton pumping in cytochrome c oxidase: Energetic requirements and the role of two proton channels. *Biochim. Biophys. Acta* **1837**, 1165–1177 (2014).
12. D. M. Popović, I. V. Leontyev, D. G. Beech, A. A. Stuchebrukhov, Similarity of cytochrome *c* oxidases in different organisms. *Proteins* **78**, 2691–2698 (2010).
13. C. von Ballmoos, P. Ädelroth, R. B. Gennis, P. Brzezinski, Proton transfer in ba_3 cytochrome *c* oxidase from *Thermus thermophilus*. *Biochim. Biophys. Acta* **1817**, 650–657 (2012).
14. M. Wikström, V. Sharma, V. R. I. Kaila, J. P. Hosler, G. Hummer, New perspectives on proton pumping in cellular respiration. *Chem. Rev.* **115**, 2196–2221 (2015).
15. M. M. Pereira, M. Santana, M. Teixeira, A novel scenario for the evolution of haem–copper oxygen reductases. *Biochim. Biophys. Acta* **1505**, 185–208 (2001).
16. J. Hemp, R. B. Gennis, Diversity of the heme–copper superfamily in archaea: Insights from genomics and structural modeling. *Results Probl. Cell Differ.* **45**, 1–31 (2008).
17. H. J. Lee, J. Reimann, Y. Huang, P. Ädelroth, Functional proton transfer pathways in the heme–copper oxidase superfamily. *Biochim. Biophys. Acta* **1817**, 537–544 (2012).
18. H. Y. Chang, J. Hemp, Y. Chen, J. A. Fee, R. B. Gennis, The cytochrome ba_3 oxygen reductase from *Thermus thermophilus* uses a single input channel for proton delivery to the active site and for proton pumping. *Proc. Natl. Acad. Sci. U.S.A.* **106**, 16169–16173 (2009).
19. T. Soulimane, G. Buse, G. P. Bourenkov, H. D. Bartunik, R. Huber, M. E. Than, Structure and mechanism of the aberrant ba_3-cytochrome *c* oxidase from *Thermus thermophilus*. *EMBO J.* **19**, 1766–1776 (2000).
20. T. Tiefenbrunn, W. Liu, Y. Chen, V. Katritch, C. D. Stout, J. A. Fee, V. Cherezov, High resolution structure of the ba_3 cytochrome *c* oxidase from *Thermus thermophilus* in a lipidic environment. *PLOS ONE* **6**, e22348 (2011).
21. V. M. Luna, Y. Chen, J. A. Fee, C. D. Stout, Crystallographic studies of Xe and Kr binding within the large internal cavity of cytochrome ba_3 from *Thermus thermophilus*: Structural analysis and role of oxygen transport channels in the heme–Cu oxidases. *Biochemistry* **47**, 4657–4665 (2008).
22. B. Chance, C. Saronio, J. S. Leigh Jr., Functional intermediates in the reaction of membrane-bound cytochrome oxidase with oxygen. *J. Biol. Chem.* **250**, 9226–9237 (1975).
23. M. Wikström, Energy-dependent reversal of the cytochrome oxidase reaction. *Proc. Natl. Acad. Sci. U.S.A.* **78**, 4051–4054 (1981).
24. G. T. Babcock, C. Varotsis, Y. Zhang, O_2 activation in cytochrome oxidase and in other heme proteins. *Biochim. Biophys. Acta* **1101**, 192–194 (1992).
25. G. T. Babcock, M. Wikström, Oxygen activation and the conservation of energy in cell respiration. *Nature* **356**, 301–309 (1992).
26. G. T. Babcock, How oxygen is activated and reduced in respiration. *Proc. Natl. Acad. Sci. U.S.A.* **96**, 12971–12973 (1999).
27. L. Weng, G. M. Baker, Reaction of hydrogen peroxide with the rapid form of resting cytochrome oxidase. *Biochemistry* **30**, 5727–5733 (1991).
28. D. A. Proshlyakov, T. Ogura, K. Shinzawa-Itoh, S. Yoshikawa, E. H. Appelman, T. Kitagawa, Selective resonance Raman observation of the "607 nm" form generated in the reaction of oxidized cytochrome *c* oxidase with hydrogen peroxide. *J. Biol. Chem.* **269**, 29385–29388 (1994).
29. D. A. Proshlyakov, M. A. Pressler, G. T. Babcock, Dioxygen activation and bond cleavage by mixed-valence cytochrome *c* oxidase. *Proc. Natl. Acad. Sci. U.S.A.* **95**, 8020–8025 (1998).
30. D. A. Proshlyakov, T. Ogura, K. Shinzawa-Itoh, S. Yoshikawa, T. Kitagawa, Microcirculating system for simultaneous determination of Raman and absorption spectra of enzymatic reaction intermediates and its application to the reaction of cytochrome *c* oxidase with hydrogen peroxide. *Biochemistry* **35**, 76–82 (1996).
31. T. Kitagawa, T. Ogura, Time-resolved resonance Raman investigation of oxygen reduction mechanism of bovine cytochrome *c* oxidase. *J. Bioenerg. Biomembr.* **30**, 71–79 (1998).
32. M. Fabian, W. W. Wong, R. B. Gennis, G. Palmer, Mass spectrometric determination of dioxygen bond splitting in the "peroxy" intermediate of cytochrome *c* oxidase. *Proc. Natl. Acad. Sci. U.S.A.* **96**, 13114–13117 (1999).
33. R. B. Gennis, Multiple proton-conducting pathways in cytochrome oxidase and a proposed role for the active-site tyrosine. *Biochim. Biophys. Acta* **1365**, 241–248 (1998).
34. M. R. A. Blomberg, P. E. M. Siegbahn, G. T. Babcock, M. Wikström, O–O bond splitting mechanism in cytochrome oxidase. *J. Inorg. Biochem.* **80**, 261–269 (2000).
35. M. R. A. Blomberg, P. E. M. Siegbahn, G. T. Babcock, M. Wikström, Modeling cytochrome oxidase: A quantum chemical study of the O–O bond cleavage mechanism. *J. Am. Chem. Soc.* **122**, 12848–12858 (2000).
36. B. C. Hill, C. Greenwood, Spectroscopic evidence for the participation of compound A (Fe_{a3}^{2+}-O_2) in the reaction of mixed-valence cytochrome *c* oxidase with oxygen at room temperature. *Biochem. J.* **215**, 659–667 (1983).
37. M. Karpefors, P. Ädelroth, A. Namslauer, Y. Zhen, P. Brzezinski, Formation of the "peroxy" intermediate in cytochrome *c* oxidase is associated with internal proton/hydrogen transfer. *Biochemistry* **39**, 14664–14669 (2000).
38. K. Oda, T. Ogura, E. H. Appelman, S. Yoshikawa, The intrinsic stability of the second intermediate following the dioxygen-bound form in the O_2 reduction by cytochrome *c* oxidase. *FEBS Lett.* **570**, 161–165 (2004).
39. B. C. Hill, C. Greenwood, The reaction of fully reduced cytochrome *c* oxidase with oxygen studied by flow-flash spectrophotometry at room temperature. Evidence for new pathways of electron transfer. *Biochem. J.* **218**, 913–921 (1984).
40. S. Han, Y.-C. Ching, D. L. Rousseau, Cytochrome *c* oxidase: Decay of the primary oxygen intermediate involves direct electron transfer from cytochrome *a*. *Proc. Natl. Acad. Sci. U.S.A.* **87**, 8408–8412 (1990).
41. M. I. Verkhovsky, J. E. Morgan, M. Wikström, Oxygen binding and activation: Early steps in the reaction of oxygen with cytochrome c oxidase. *Biochemistry* **33**, 3079–3086 (1994).
42. P. Ädelroth, M. Ek, P. Brzezinski, Factors determining electron-transfer rates in cytochrome *c* oxidase: Investigation of the oxygen reaction in the *R. sphaeroides* enzyme. *Biochim. Biophys. Acta* **1367**, 107–117 (1998).
43. A. Sucheta, I. Szundi, Ó. Einarsdóttir, Intermediates in the reaction of fully reduced cytochrome *c* oxidase with dioxygen. *Biochemistry* **37**, 17905–17914 (1998).
44. S. Graf, O. Fedotovskaya, W.-C. Kao, C. Hunte, P. Ädelroth, M. Bott, C. von Ballmoos, P. Brzezinski, Rapid electron transfer within the III-IV supercomplex in *Corynebacterium glutamicum*. *Sci. Rep.* **6**, 34098 (2016).
45. L. Salomonsson, K. Faxén, P. Ädelroth, P. Brzezinski, The timing of proton migration in membrane-reconstituted cytochrome *c* oxidase. *Proc. Natl. Acad. Sci. U.S.A.* **102**, 17624–17629 (2005).
46. M. Karpefors, P. Ädelroth, A. Aagaard, I. A. Smirnova, P. Brzezinski, The deuterium isotope effect as a tool to investigate enzyme catalysis: Proton-transfer control mechanisms in cytochrome *c* oxidase. *Isr. J. Chem.* **39**, 427–437 (1999).
47. C. von Ballmoos, R. B. Gennis, P. Ädelroth, P. Brzezinski, Kinetic design of the respiratory oxidases. *Proc. Natl. Acad. Sci. U.S.A.* **108**, 11057–11062 (2011).
48. M. R. A. Blomberg, P. E. M. Siegbahn, Quantum chemistry applied to the mechanisms of transition metal containing enzymes—Cytochrome *c* oxidase, a particularly challenging case. *J. Comput. Chem.* **27**, 1373–1384 (2006).
49. M. R. A. Blomberg, T. Borowski, F. Himo, R.-Z. Liao, P. E. M. Siegbahn, Quantum chemical studies of mechanisms for metalloenzymes. *Chem. Rev.* **114**, 3601–3658 (2014).
50. M. R. A. Blomberg, P. E. M. Siegbahn, Quantum chemistry as a tool in bioenergetics. *Biochim. Biophys. Acta* **1797**, 129–142 (2010).
51. S. A. Siletsky, I. Belevich, A. Jasaitis, A. A. Konstantinov, M. Wikström, T. Soulimane, M. I. Verkhovsky, Time-resolved single-turnover of ba_3 oxidase from *Thermus thermophilus*. *Biochim. Biophys. Acta* **1767**, 1383–1392 (2007).
52. C. Koutsoupakis, O. Kolaj-Robin, T. Soulimane, C. Varotsis, Probing protonation/deprotonation of tyrosine residues in cytochrome ba_3 oxidase from *Thermus*

thermophilus by time-resolved step-scan Fourier transform infrared spectroscopy. *J. Biol. Chem.* **286**, 30600–30605 (2011).
53. M. Oliveberg, P. Brzezinski, B. G. Malmström, The effect of pH and temperature on the reaction of fully reduced and mixed-valence cytochrome *c* oxidase with dioxygen. *Biochim. Biophys. Acta* **977**, 322–328 (1989).
54. M. R. A. Blomberg, Mechanism of oxygen reduction in cytochrome c oxidase and the role of the active site tyrosine. *Biochemistry* **55**, 489–500 (2016).
55. M. Brändén, H. Sigurdson, A. Namslauer, R. B. Gennis, P. Ädelroth, P. Brzezinski, On the role of the K-proton transfer pathway in cytochrome *c* oxidase. *Proc. Natl. Acad. Sci. U.S.A.* **98**, 5013–5018 (2001).
56. C. von Ballmoos, P. Lachmann, R. B. Gennis, P. Ädelroth, P. Brzezinski, Timing of electron and proton transfer in the ba_3 cytochrome *c* oxidase from *Thermus thermophilus*. *Biochemistry* **51**, 4507–4517 (2012).
57. I. Szundi, C. Funatogawa, J. A. Fee, T. Soulimane, Ó. Einarsdóttir, CO impedes superfast O_2 binding in ba_3 cytochrome oxidase from *Thermus thermophilus*. *Proc. Natl. Acad. Sci. U.S.A.* **107**, 21010–21015 (2010).
58. A. Giuffrè, E. Forte, G. Antonini, E. D'Itri, M. Brunori, T. Soulimane, G. Buse, Kinetic properties of ba_3 oxidase from *Thermus thermophilus*: Effect of temperature. *Biochemistry* **38**, 1057–1065 (1999).
59. G. V. Isaksen, J. Åqvist, B. O. Brandsdal, Protein surface softness is the origin of enzyme cold-adaptation of trypsin. *PLOS Comput. Biol.* **10**, e1003813 (2014).
60. L. M. Blomberg, M. R. A. Blomberg, P. E. M. Siegbahn, A theoretical study on the binding of O_2, NO and CO to heme proteins. *J. Inorg. Biochem.* **99**, 949–958 (2005).
61. I. Smirnova, H.-Y. Chang, C. von Ballmoos, P. Ädelroth, R. B. Gennis, P. Brzezinski, Single mutations that redirect internal proton transfer in the ba_3 oxidase from *Thermus thermophilus*. *Biochemistry* **52**, 7022–7030 (2013).
62. I. Smirnova, J. Reimann, C. von Ballmoos, H.-Y. Chang, R. B. Gennis, J. A. Fee, P. Brzezinski, P. Ädelroth, Functional role of Thr-312 and Thr-315 in the proton-transfer pathway in ba_3 cytochrome *c* oxidase from *Thermus thermophilus*. *Biochemistry* **49**, 7033–7039 (2010).
63. Y. Chen, L. Hunsicker-Wang, R. L. Pacoma, E. Luna, J. A. Fee, A homologous expression system for obtaining engineered cytochrome ba_3 from *Thermus thermophilus* HB8. *Protein Exp. Purif.* **40**, 299–318 (2005).
64. J. A. Keightley, B. H. Zimmermann, M. W. Mather, P. Springer, A. Pastuszyn, D. M. Lawrence, J. A. Fee, Molecular genetic and protein chemical characterization of the cytochrome ba_3 from *Thermus thermophilus* HB8. *J. Biol. Chem.* **270**, 20345–20358 (1995).
65. C. Rydström Lundin, C. von Ballmoos, M. Ott, P. Ädelroth, P. Brzezinski, Regulatory role of the respiratory supercomplex factors in *Saccharomyces cerevisiae*. *Proc. Natl. Acad. Sci. U.S.A.* **113**, E4476–E4485 (2016).
66. M. L. Björck, S. Zhou, C. Rydström Lundin, M. Ott, P. Ädelroth, P. Brzezinski, Reaction of *S. cerevisiae* mitochondria with ligands: Kinetics of CO and O_2 binding to flavohemoglobin and cytochrome *c* oxidase. *Biochim. Biophys. Acta* **1858**, 182–188 (2017).
67. M. R. A. Blomberg, P. E. M. Siegbahn, How cytochrome c oxidase can pump four protons per oxygen molecule at high electrochemical gradient. *Biochim. Biophys. Acta* **1847**, 364–376 (2015).
68. A. D. Becke, Density-functional thermochemistry. III. The role of exact exchange. *J. Chem. Phys.* **98**, 5648–5652 (1993).
69. M. Reiher, O. Salomon, B. A. Hess, Reparameterization of hybrid functionals based on energy differences of states of different multiplicity. *Theor. Chem. Acc.* **107**, 48–55 (2001).
70. S. Grimme, J. Antony, S. Ehrlich, H. Krieg, A consistent and accurate ab initio parametrization of density functional dispersion correction (DFT-D) for the 94 elements H-Pu. *J. Chem. Phys.* **132**, 154104 (2010).
71. Jaguar 7.6 (Schrödinger-LLC, New York, 2009).
72. M. R. A. Blomberg, P. E. M. Siegbahn, Improved free energy profile for reduction of NO in cytochrome c dependent nitric oxide reductase (cNOR). *J. Comput. Chem.* **37**, 1810–1818 (2016).

Acknowledgments: The wild-type *T. thermophilus* strain was obtained from R. B. Gennis at the University of Illinois at Urbana-Champaign. **Funding:** These studies were supported by grants from the Knut and Alice Wallenberg Foundation (KAW 2013.0006) and the Swedish Research Council (2014-4306 and 2015-04512). **Author contributions:** F.P. and C.v.B. (N.G. initially supervised F.P.) performed experiments and evaluated experimental data. M.R.A.B. performed calculations. P.B., P.Ä., and C.v.B. interpreted the data. P.B. and M.R.A.B. (the part on calculations) wrote the manuscript. All authors commented on the text, format of presentation, and data evaluation and interpretation. **Competing interests:** The authors declare that they have no competing interests. **Data and materials availability:** All data needed to evaluate the conclusions in the paper are present in the paper. Additional data related to this paper may be requested from the authors.

Submitted 26 January 2017
Accepted 20 April 2017
Published 16 June 2017
10.1126/sciadv.1700279

Citation: F. Poiana, C. von Ballmoos, N. Gonska, M. R. A. Blomberg, P. Ädelroth, P. Brzezinski, Splitting of the O–O bond at the heme-copper catalytic site of respiratory oxidases. *Sci. Adv.* **3**, e1700279 (2017).

ScienceAdvances

Splitting of the O–O bond at the heme-copper catalytic site of respiratory oxidases

Federica Poiana, Christoph von Ballmoos, Nathalie Gonska, Margareta R. A. Blomberg, Pia Ädelroth and Peter Brzezinski

Sci Adv **3** (6), e1700279.
DOI: 10.1126/sciadv.1700279